PCCP

ROYAL SOCIETY OF CHEMISTRY

PAPER

View Article Online
View Journal | View Issue

Cite this: *Phys. Chem. Chem. Phys.*, 2021, **23**, 4365

Structure-directed formation of the dative/covalent bonds in complexes with $C_{70}\cdots$piperidine†

Rabindranath Lo, ‡[ab] Maximilián Lamanec,‡[ac] Weizhou Wang, [d] Debashree Manna,[ab] Aristides Bakandritsos, [be] Martin Dračínský, [a] Radek Zbořil, [abef] Dana Nachtigallová*[ab] and Pavel Hobza *[ab]

Received 4th December 2020,
Accepted 4th February 2021

DOI: 10.1039/d0cp06280d

rsc.li/pccp

The combined experimental-computational study has been performed to investigate the complexes formed between C_{70} carbon allotrope and piperidine. The results of FT-IR, H-NMR, and C-NMR measurements, together with the calculations based on the DFT approach and molecular dynamics simulations, prove the existence of dative/covalent bonding in $C_{70}\cdots$piperidine complexes. The dative bond forms not only at the region of five- and six-membered rings, observed previously with C_{60}, but also at the region formed of six-membered rings. The structure, *i.e.*, nonplanarity, explains the observed dative bond formation. New findings on the character of interaction of secondary amines with C_{70} bring new aspects for the rational design of modified fullerenes and their applications in electrocatalysis, spintronics, and energy storage.

1. Introduction

Fullerene, ball-shaped compounds composed of five- and six-membered rings, their functionalized derivatives, and supramolecular assemblies are nowadays widely investigated systems for their promising applications in medicine and material chemistry (see the most recent reviews in ref. 1–6). Compared to the most abundant C_{60}, the chemistry of C_{70} is less known, although its adducts' performance, *e.g.*, in the solar cells, sometimes appears superior to their C_{60}-analogues.[7] Despite their similar physical and chemical properties[8–11] structural differences between C_{60} and C_{70} have resulted in frequently observed diverse reactivity (see ref. 12 and discussion below). Unlike the spherically symmetric C_{60} possessing I_h symmetry with all carbon atoms equivalent, C_{70} has a less symmetrical structure of D_{5h} with five different types of carbon atoms[13] (see Scheme 1). A vast number of studies on the addition reactions with C_{70}, including the addition of secondary amines, under various conditions, have been reported,[14–25] showing significant regioselectivity owing to differences in reactivity of the polar and equatorial regions of the C_{70} structure.

High reactivity towards addition reactions stems from a distortion of the π-conjugation from planarity, decreasing p-orbital contributions involved to the π-bonds and increasing s-orbital contribution to sp^2 carbon atoms, respectively; hence, there is a significant decrease of aromaticity character of these spherical carbon allotropes and enhanced capability to accept electrons.[26] Besides the widely studied addition reaction mechanism, as demonstrated for C_{70} in the above references, electron-accepting properties of fullerenes proved to facilitate also binding of nucleophilic agents, such as the secondary amine, piperidine (pip), by the N→C dative/covalent bond (further abbreviated as N→C bond). As shown in ref. 27, dative bond (DB) complexes can coexist with non-covalent complexes of piperidine and cage-shaped carbon allotropes. Computational studies on pip complexes with C_{20}, formed exclusively by five-member rings, and with C_{60}, with five- and six-member rings, demonstrated the stronger binding character of the former complexes. The failure to form the N→C bond in non-planar carbon allotropes formed exclusively by six-member rings, such as carbon nanotubes with different diameters, led to the conclusion that the presence of five-membered rings is of crucial importance in binding. Such prediction was based on a larger aromaticity decrease in

[a] *Institute of Organic Chemistry and Biochemistry, Czech Academy of Sciences, Flemingovo Náměstí 542/2, 16000 Prague, Czech Republic. E-mail: pavel.hobza@uochb.cas.cz, dana.nachtigallova@uochb.cas.cz*
[b] *CATRIN, Palacký University, Šlechtitelů 27, 78371 Olomouc, Czech Republic*
[c] *Department of Physical Chemistry, Palacký University Olomouc, Tr. 17 listopadu 12, 771 46 Olomouc, Czech Republic*
[d] *College of Chemistry and Chemical Engineering, and Henan Key Laboratory of Function-Oriented Porous Materials, Luoyang Normal University, Luoyang 471934, China*
[e] *Regional Centre of Advanced Technologies and Materials, Palacký University, Olomouc, Šlechtitelů 27, 78371, Czech Republic*
[f] *Nanotechnology Centre, VŠB-Technical University of Ostrava, 17. Listopadu 2172/15, 708 00 Ostrava-Poruba, Czech Republic*

† Electronic supplementary information (ESI) available. See DOI: 10.1039/d0cp06280d

‡ Both authors contributed equally and can be considered as the first author.

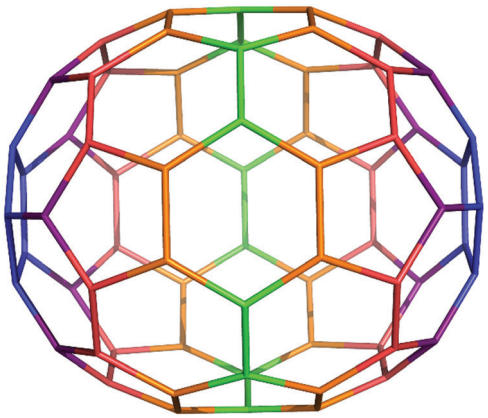

Scheme 1 Illustration of five unequal sites of C_{70} differentiated by colors. The sites considered for piperidine binding are indicated by blue (A-sites), red (B-sites), and green (C-sites), respectively.

five-member rings, which tend to localize double bonds, thus preventing π-electrons from conjugation.[28,29]

To further explore the structural requirements to form the N→C bond in cage-shaped carbon allotropes, the next most abundant C_{70} was considered in the present study employing a combination of IR and NMR spectroscopies and computational modeling, including interaction and binding free energy calculations and molecular dynamics simulations of $C_{70}\cdots(pip)_n$ complexes. The calculations consider three carbon-sites (Scheme 1): (i) sites A and B located at five- and six-member rings and differing by their localization within C_{70} and (ii) site C located within the structure fragments formed solely by six-member rings. The former two sites are similar to the carbon site of C_{60}. To rationalize differences in N→C bond strengths, the local electrophilicity index calculations, using Fukui functions[30,31] were performed. These functions provide atom-specific information on the propensity to undergo electrophilic or nucleophilic attack.[32] Recently, Fukui indices were used extensively, *e.g.*, for a successful rationalization of favorable and competing reactive sites in fullerenes.[33–35]

The present results show different stabilities of $C_{70}\cdots(pip)_{1,2}$ complexes depending on the type of carbon site involved in the reaction. A stronger dative bond is formed at A- and B-sites, *i.e.*, located at five- and six-member rings, while binding to C-site formed solely by six-member rings is weaker. The significant out-of-plane nonplanarity explained the unexpected formation of the dative bond in the latter region. When the entropy is considered, only the former sites' complexes remain stable up to 300 K. Existence of the N→C bond is confirmed by IR and NMR measurements. The presented results confirm the regioselectivity observed for the addition mechanism and provide useful information on structure-specific functionalization.

2. Methods

2.1. Calculations

Calculations were performed using the dispersion-corrected-DFT method, employing the PBE0-D3[36,37] functional with Becke–Johnson damping (BJ)[38] and def2-TZVPP[39] basis set, whose reliability has been verified in our previous paper.[27] All interactions are described in terms of interaction and binding free energies at 298 K; zero-point energies were included. The free energy calculations, performed at the PBE0-D3/def2-TZVPP level, were calculated using the Gaussian 09[40] program package. The solvent effects were described *via* the COSMO solvation model,[41] with the dielectric constant value of 5.9. The nucleus-independent chemical shift (NICS) calculations were carried out at wB97XD/def2-TZVP[42,43] level, using the PBE0-D3 optimized geometries with gauge-invariant atomic orbitals (GIAO).[44,45] The reliability of this method for the chemical shifts' calculations in C_{70} was investigated previously.[46]

The systems' stability is defined by two terms, the intrinsic (ΔE^{INTR}) and total (ΔE) interaction energies. ΔE^{INTR} is defined as a difference between energy of the optimized complex and the sum of subsystem energies calculated at the complex geometries. ΔE includes the deformation energies (ΔE^{def}) obtained as a difference of the subsystem energies calculated at the complex's optimized geometry and the equilibrium geometries of isolated subsystems.

The MP2 calculations of ΔE^{INTR} have been performed using the Psi4[47] code.

To obtain a more realistic description of C_{70} solvation, the molecular dynamics (MD) simulations were performed. These simulations use the AM1-D semiempirical approach since the previously used DFT method is prohibitive due to the system's size. We have shown that in terms of stabilization energies and the minimum characterization on $C_{60}\cdots(pip)_n$ complexes, this approach gives the best agreement with respect to the benchmark calculations among other semiempirical methods.[27]

The MD simulations have been performed with the AM1 method implemented in Mopac 2016[48] using the Cuby4 framework[49] with added D3[50] dispersion. The heating of systems was realized from 0 to 300 K by 3000 steps. MD 0.1 ns simulations were carried out at 300 K using the Berendsen thermostat.[51] Domain-based Local Pair Natural Orbital-CCSD(T) (DLPNO-CCSD(T))[52,53] the single-point calculations were performed for the DFT optimized geometries using def2-SVP basis set. An energy decomposition scheme for the total interaction energy within the DLPNO framework, known as local energy decomposition (LED),[54] was used for detailed analyses of the interaction energies.

2.2. IR spectroscopy

A paste of C_{70} (4 mg) and *ca.* 20 μl of piperidine was mixed in a mortar. It was then ground with a pestle for 5 minutes and placed with a pipette on the ZnSe crystal of the FT-IR instrument. The spectra were collected immediately (C_{60}-P1 sample) and after a few minutes (C_{60}-P2 sample) to let pip molecules evaporate until the IR signal was enriched with the vibrations from the C_{60}–pip complex.

FT-IR spectra were recorded on an iS5 FTIR spectrometer (Thermo Nicolet) using the Smart Orbit ZnSe ATR accessory. The pastes or liquid piperidine were placed on the ZnSe crystal, and the spectra were acquired by summing 32 scans with

nitrogen gas flow through the accessory. Background spectra were collected under identical conditions.

2.3. NMR spectroscopy

Solution-state NMR spectra were recorded on Bruker Avance 600 (^{1}H at 600 MHz, ^{13}C at 151 MHz) spectrometer in deuterated 1,2-dichlorobenzene. The spectra were referenced to the residual solvent signal (the highest-chemical-shift signals at 7.40 ppm for ^{1}H and 132.60 ppm for ^{13}C). All chemicals were purchased from Sigma-Aldrich and were used without further purification. Fullerene C_{70} (11 mg) was dissolved in 1,2-dichlorobenzene-d4 (550 μL) with sonication and vigorous mixing. After the proton and carbon spectra acquisition, piperidine (35 μL) was added, and the proton and carbon spectra of the mixture were measured.

3. Results and discussion

3.1. Interaction energies

C_{70}···pip. Fig. 1 displays the structures of C_{70}···pip complexes formed at A, B, and C sites of C_{70} optimized using the PBE0-D3/def2-TZVPP approach. The optimization procedure located two types of minima, formed by the interaction between C(C_{70}) and N(pip): the vdW complexes which interact *via* C···N tetrel bond[55] with the bond lengths of 2.9–3.1 Å and the DB complexes interacting *via* N→C bond with bond lengths of about 1.6 Å. The calculations show that the vdW complex type can exist on all (A, B, and C) sites with very similar stabilities of 5.2–5.5 kcal mol^{-1}. In all cases, almost identical values of ΔE and ΔE^{INTR} show negligible deformation energies, less than 0.1 kcal mol^{-1} (see also Table 1 for the deformation energies). The results obtained for DB structures provide a less uniform picture. The optimization procedures found the stable minima at A and B sites, located at the intersection of five- and six-member rings. Such a complex does not form at the all-benzoid C site. Both ΔE^{INTR} values and N→C bond distances indicate stronger interaction at the A site. Although the ΔE^{INTR} values of localized DB structures are significantly larger than their vdW counterparts, large deformation energies make them only weakly bound (site A, −2.6 kcal mol^{-1}) or unstable (site B, +1.0 kcal mol^{-1}).

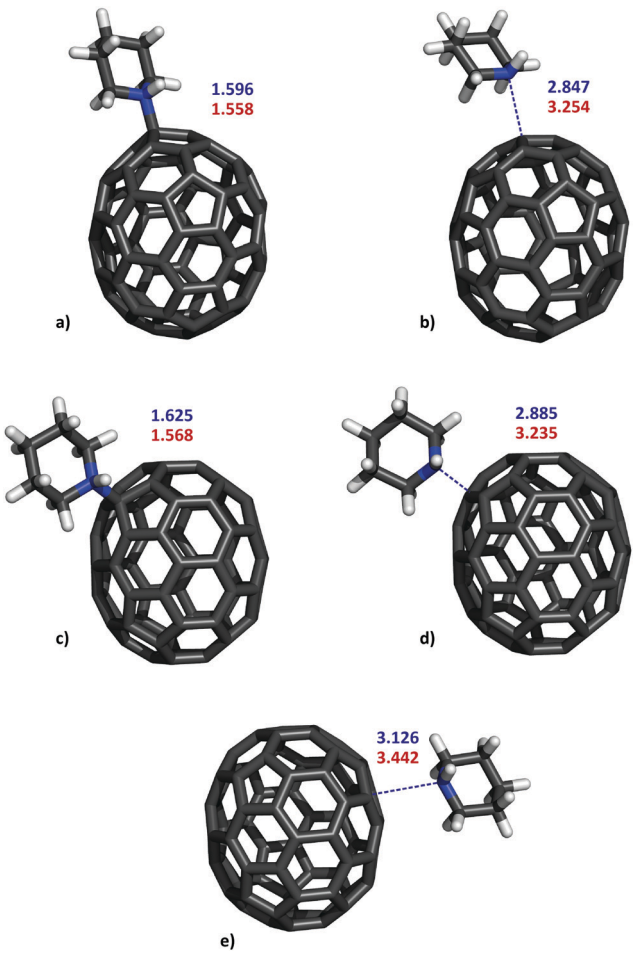

Fig. 1 The minima of C_{70}···pip: (a) DB and (b) vdW complexes at site A, (c) DB and (d) vdW complex at site B, and (e) vdW complexes at site C calculated at the PBE0-D3BJ/def2-TZVPP level. The C_{70}···pip distances are given in Å (gas phase: dark blue, solvent phase: red).

Table 1 Total DFT interaction energies (ΔE), deformation energies (ΔE^{Def}), and intrinsic interaction energies (ΔE^{INTR}) calculated at the PBE0-D3 and MP2 levels using the def2-TZVPP basis set for DFT and cc-pVQZ for MP2. In brackets are dispersion parts of ΔE^{INTR} calculated from Grimme's DFT-D3 correction. All values are in kcal mol^{-1}

		PBE0-D3			
	Site	ΔE	ΔE^{INTR}	ΔE^{Def}	ΔE^{INTR}(MP2)
C_{70}···pip					
vdW complexes	A	−5.3	−5.3(−4.9)	0.0	−7.4
	B	−5.2	−5.3(−4.9)	0.1	−7.3
	C	−5.5	−5.5(−4.9)	0.0	−7.8
DB complexes	A	−2.6	−20.1(−7.8)	17.5	−18.3
	B	+1.0	−15.3(−7.9)	16.3	−12.1
C_{70}···$(pip)_2$					
vdW complexes	B	−8.8	−10.2(−9.7)	1.4	−13.9
	C	−8.8	−9.9(−9.7)	1.1	−14.3
DB complexes	A	−16.0	−40.1(−11.6)	24.0	−40.1
	B	−12.2	−35.6(−12.1)	23.4	−34.2
	C	−4.4	−29.7(−13.0)	25.4	−31.0

C_{70}···$(pip)_2$. Binding of $(pip)_2$ provides a different picture of both DB and vdW complexes' stabilities. Fig. 2 and Table 1 display their structures and interaction energies. The interaction energies are calculated with respect to $(pip)_2$ in which the inner and outer pips bind *via* N→C bond to C_{70} and NH (inner)···N (outer) motif, respectively. Contrary to the binding of pip monomer, the vdW complexes formed at B and C sites only; all attempts to localize vdW minimum at the A site resulted in DB structures. For vdW complexes, the calculated ΔE^{INTR} and ΔE values are almost identical, and the values of their deformation energies almost negligible. Interaction energies and C–N distances reveal stronger interaction in C_{70} complexes with pip dimers than their corresponding monomer counterparts. Unlike C_{70}···pip, stable DB complexes with $(pip)_2$ formed at all carbon sites of C_{70}. As in monomer, the ΔE^{INTR} values are significantly larger, by 20–25 kcal mol^{-1}, for DB.

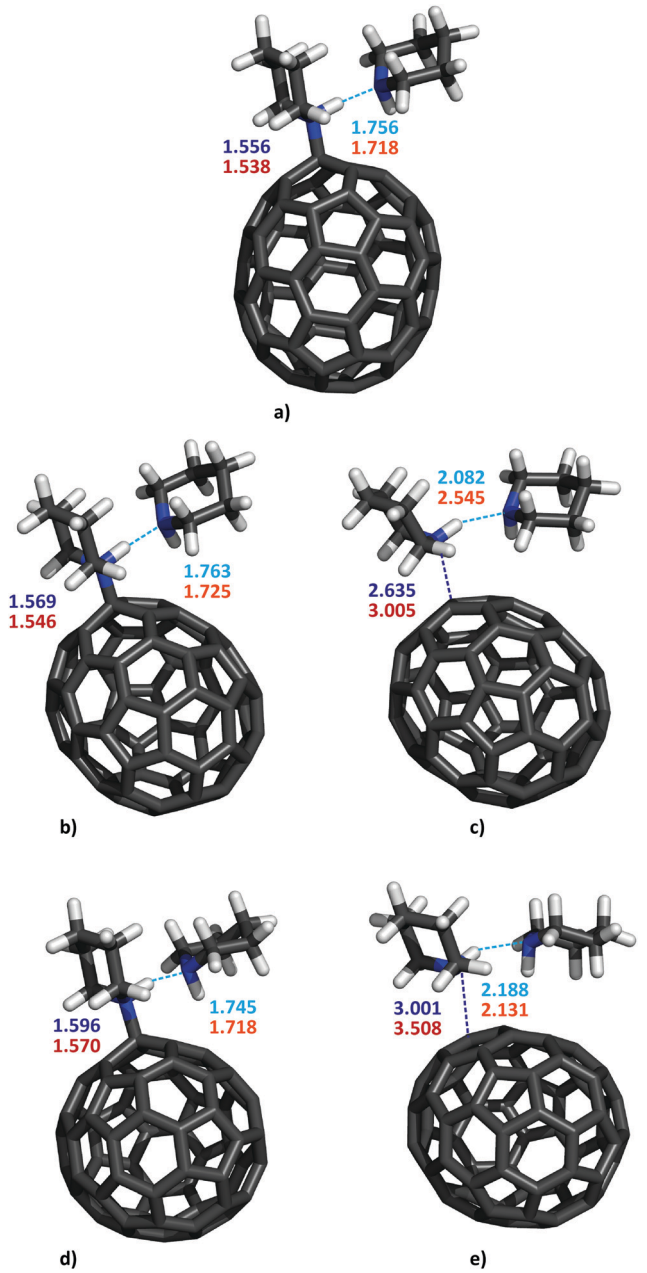

Fig. 2 The minima of $C_{70}\cdots(pip)_2$: the DB complexes at the A-site (a) and B-site (b); the vdW complex at B-site (c), the DB complex at C-site (d), and the vdW complex at the C-site (e). The structures are optimized at the PBE0-D3BJ/def2-TZVPP level. The distances are given in Å (gas phase: blue, solvent phase: red).

Besides, C–N distances in $C_{70}\cdots(pip)_2$ and N–H distances within $(pip)_2$ shorten by 1.0–1.4 Å and by 0.3 Å, respectively, reflecting the strengthening of both interactions in the complexes. Substantially larger stabilities of DB in $C_{70}\cdots(pip)_2$ than that of $C_{70}\cdots$pip, as well as shorter N–C bond lengths (see Fig. 1 and 2 and Table 1) suggest the stabilization due to cascade outer pip → inner pip → C_{70} charge-transfer, which results in strengthening of N → C dative bond. The natural bond orbital (NBO) analysis reveals a substantial charge transfer (0.67 e) from the pip dimer to C_{70}. A similar effect, *i.e.*, the hydrogen bond strengthening of the dative bond, was observed in our previous studies on the $C_{60}\cdots(pip)_n$ complexes[27] and can be viewed as a subclass of non-covalent cooperativity.[56,57]

The changes in the molecular electrostatic potential of C_{70} and pip complexes (see Fig. S1, ESI†) demonstrate different characters of the interactions. ESP of isolated C_{70} forms small, slightly positively charged islands located on top of the five- and six-membered rings. Upon the complexation with a single pip, the electron density transfers from pip to C_{70} resulting in significantly negative ESP values on the C_{70} region opposite to the pip binding site. These changes are further pronounced in the DB complex with pip dimer.

An electron-dense C_{70} can strengthen the host–guest complex stability when the ellipsoidal guest C_{70} forms a Saturn-shaped complex with a macrocyclic host molecule.[58] As the CH$\cdots\pi$ interactions play an important role in these host–guest complex types, the DB complex of C_{70} should be a better guest molecule than isolated C_{70}.

From an electrochemical perspective, an efficient charge transfer process requires substantial differences in the redox properties, in particular, redox potentials (estimated using adiabatic electron affinities (AEA)),[59] of the isolated C_{70} and DB complex. The calculated AEA of the C_{70} and $C_{70}\cdots$pip are 2.62 eV and 2.18 eV, respectively, showing decreasing in the electron-accepting ability upon complexation with pip.

The deformation energies of about 25 kcal mol^{-1} for all sites significantly affect DB overall stability, reordering DB and vdW relative stabilities at the C site.

The observed energy balance between the vdW and DB complexes of $C_{70}\cdots$pip and $C_{70}\cdots(pip)_2$ for different sites reveal different potentials for formation, *i.e.*, the increasing probability of DB complex formation in the C → B → A sequence and the opposite trend for vdW complex formation. This phenomenon is discussed in paragraph 3.6.

Calculated DFT-D3 corrections (Table 1) demonstrate the role of dispersion interactions in complex stabilities, showing their significant contributions in both binding types. In particular, the dispersion energy dominates the interaction energies in the vdW complexes and contributes to the total interaction energies of the DB complexes by 30–50%, respectively. We have performed local energy decomposition (LED) analysis at the DLPNO-CCSD(T)[60,61] level (Table S1, ESI†). Stabilizing electrostatic as well as destabilizing exchange-repulsion energies have a small contribution to the stabilization energy. The DLPNO-CCSD(T) intrinsic energy is in reasonable agreement with that calculated at the DFT level. Table 1 also lists the results of ΔE^{INTR} calculations obtained at the MP2/cc-pVQZ level, showing agreement with PBE0-D3/def2-TZVPP results in the complexes' relative stabilities. The ΔE^{INTR} values do not differ by more than 10% for the majority of structures. Significant overstabilization at the MP2 level for vdW, which accounts for 40–45%, demonstrates the well-known overestimation of the dispersion interactions in the MP2 method. Nevertheless, the present results and benchmarking results with the highly accurate CCSD(T) method performed on smaller fullerenes[27] justify the reliability of the DFT-based

Table 2 Thermodynamic characteristics (in kcal mol^{-1}, T = 298 K) for the formation of $C_{70}\cdots$pip and $C_{70}\cdots pip_2$ complexes calculated at PBE0-D3BJ/def2-TZVPP level. The solvent phase results are given in parenthesis

	Site	ΔE	ΔG	ΔH	$-T\Delta S$
$C_{70}\cdots$pip					
vdW complexes	A	−5.3 (−3.9)	4.6 (5.5)	−4.0 (−2.6)	8.6 (8.1)
	B	−5.2 (−4.0)	4.2 (5.5)	−3.9 (−2.7)	8.1 (8.2)
	C	−5.5 (−4.2)	3.5 (5.0)	−4.2 (−2.9)	7.7 (7.8)
DB complexes	A	−2.6 (−9.6)	13.0 (6.3)	−0.3 (−7.0)	13.3 (13.4)
	B	1.0 (−5.7)	16.3 (10.1)	3.2 (−3.2)	13.2 (13.3)
$C_{70}\cdots(pip)_2$					
vdW complexes	B	−8.8 (−6.0)	4.2 (5.5)	−8.1 (−5.4)	12.3 (10.8)
	C	−8.8 (−7.1)	0.9 (3.2)	−7.5 (−5.7)	8.4 (8.9)
DB complexes	A	−16.0 (−19.6)	1.8 (−1.8)	−13.7 (−17.3)	15.5 (15.5)
	B	−12.2 (−15.8)	5.6 (1.6)	−10.0 (−13.6)	15.6 (15.2)
	C	−4.4 (−5.7)	12.9 (11.7)	−2.4 (−3.7)	15.3 (15.4)

approach in this case and its use for further studies on $C_{70}\cdots(pip)_n$ complexes.

We quantify the local aromaticities of 5- and 6-membered rings of the $C_{70}\cdots$pip and $C_{70}\cdots(pip)_2$ DB complexes by NICS(0)$_{zz}$ indexes calculated at the ring centroids[62] and compare them with those of the isolated C_{70} (Fig. S2 and Table S2, ESI†). The aromaticity of the 5-membered rings in the polar region increases upon complex formation with pip. The NICS(0)zz values of the 5-membered rings in the equatorial region in DB complexes significantly change and become antiaromatic.

3.2. Binding free energies

Further insight to the $C_{70}\cdots$pip and $C_{70}\cdots(pip)_2$ complex formation is provided by the calculations of the free energy (ΔG) at 298 K, performed at the PBE0-D3/def2-TZVPP level (Table 2). Insertion of entropy effects results in positive ΔG values, which, however, does not rule out the existence of the complex in pip solvent. The solvent pip molecules can stabilize the complex *via* dative and non-covalent bonds. In the continuum solvent model, the $C_{70}\cdots(pip)_2$ complex at A-site has a negative ΔG value of −1.8 kcal mol^{-1} (Table 2). Thus, $C_{70}\cdots(pip)_2$ complex with $(pip)_2$ attached to the A-site *via* dative bond is the most likely to be formed and detectable in the experiment.

3.3. MD simulations

To provide a more realistic model picture of the complex formation in the piperidine solvent, the MD simulations in the piperidine droplet (26 solvent molecules) were performed. The systems' size prohibits using the DFT approach even with the limited 6-31G* basis set.

Table 3 compares results on the relative stabilities of $C_{70}\cdots(pip)_{1,2}$ complexes obtained with the PBE0-D3/def2-TZVPP and MP2/cc-pVQZ and AM1-D methods. The AM1-D approach reproduces the ΔE and ΔE^{INTR} values of vdW complexes with an excellent agreement. Although the interaction energies of $C_{70}\cdots(pip)_{1,2}$ are overestimated at this level, AM1-D still predicts larger stabilities of $C_{70}\cdots(pip)_2$, with the complexation at C-site being the least probable.

Two minima, with one or two pip molecules interacting *via* N→C bond (S1 and S2, Fig. 3) with A-sites of C_{70}, were found. Note that the dative bond is formed at A-sites even if the optimization procedure started from the structure with N→C bond at C-site. The S1 structure, with one N→C bond, is by 10 kcal mol^{-1} less stable than the S2 system.

The molecular dynamics simulations starting from the S1 and S2 structures and running for 100 000 MD steps (*i.e.*, total simulation time 100 ps) at 298 K confirmed the existence of one and two N→C bonds complex. During the molecular dynamics run, three (S1 structure) and four (S2 structure) pip molecules escape from the surrounding shell.

3.4. FT-IR spectra

Fig. 4 shows the FT-IR spectra of C_{70} and its mixture with piperidine solvent after the evaporation of some excess amount of unbound piperidine molecules (labeled C_{70}-P1 and C_{70}-P2, respectively). For the sake of comparison, the FT-IR spectra of C_{60} with the piperidine solvent (C_{60}-P2 discussed previously (ref. 27)) are also included.[27] In addition to the collective band at 1000–1200 cm^{-1} previously assigned to the C–N bond and skeletal –C–N–C stretchings[63,64] due to unbound piperidine molecules, a new band appears at 983 cm^{-1}. A similar situation was also observed in the C_{60}-P2 spectrum (see also ref. 27).

Table 3 Comparison of the total interaction energies (ΔE, kcal mol^{-1}) and intrinsic interaction energies (ΔE^{INTR}) calculated at the PBE0-D3, MP2, and AM1-D methods

	Site	ΔE (DFT)	ΔE (AM1-D)	ΔE^{INTR} (DFT)	ΔE^{INTR} (MP2)	ΔE^{INTR} (AM1-D)
$C_{70}\cdots$pip						
vdW complexes	A	−5.3	−6.5	−5.3	−7.4	−6.5
	B	−5.2	−6.7	−5.3	−7.3	−6.7
	C	−5.5	−7.1	−5.5	−7.8	−7.1
DB complexes	A	−2.6	−9.8	−20.1	−18.3	−31.1
	B	+1.0	−9.8	−15.3	−12.1	−32.0
$C_{70}\cdots(pip)_2$						
vdW complexes	B	−8.8	−11.3	−10.2	−13.9	−12.3
	C	−8.8	−11.2	−9.9	−14.3	−12.4
DB complexes	A	−16.0	−18.7	−40.1	−40.1	−42.3
	B	−12.2	−19.0	−35.6	−34.2	−47.4
	C	−4.4	−6.1	−29.7	−31.0	−34.6

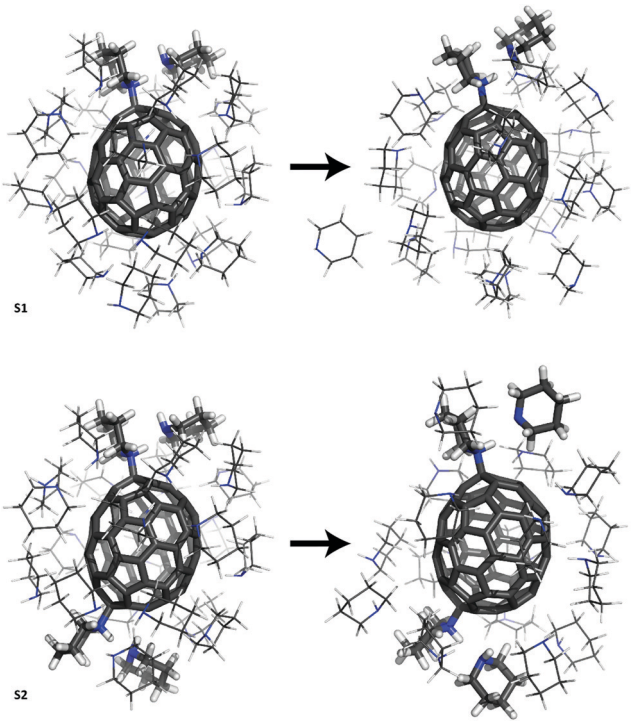

Fig. 3 The mixture of C_{70} with 26 piperidine molecules with one (S1) and two (S2) dative bonds formed in the minima structures (left) obtained in the optimization at the AM1-D level. The structures on the right side are after 0.1 ns MD AM1-D simulation.

The calculations (see Table S3 and Fig. S3, ESI†) interpret this band as a result of the asymmetric stretch (938 cm^{-1}, intensity 73 km mol^{-1}) of the newly formed N→C bond in C_{70}–$(pip)_2$ complex. Calculated symmetric stretch located at 880 cm^{-1} is also present in the C_{70}-P2 spectrum, similar to the C_{60}-P2 spectrum.

The N–H bending vibrations are expected in the spectral region of 1500 and 1650 cm^{-1}. The spectrum of unbound piperidine is consistent with these bands' negligible intensities calculated for $(pip)_{2,3}$ complexes in the previous study.[27] Compared to the C_{60}-P2 spectrum, with one clear band at 1540 cm^{-1} due to the N-H bending mode of the inner piperidine (with the N atom is involved in bond with C_{60}[27]), two bands at 1540 and 1630 cm^{-1} appear in the spectra of C_{70}-P2. Assignment of these bands relies on the (pip)2 bound calculations at three different structural motifs (A, B, and C), giving the N–H bending vibrations frequencies at 1565, 1568, and 1535 cm^{-1} at A-, B-, and C-sites, respectively. Besides, few low-intensity peaks of N–H bending vibrations appeared in the region of 1613–1624 cm^{-1} (Table S3, ESI†).

The spectral region of 2700–3000 cm^{-1} and higher than 3000 cm^{-1} correspond to C–H and N–H stretching vibrations, respectively. (Fig. 4b). The former bands are retained without changes, while an intensity depletion of the later bands upon pip evaporation indicates a decreased number of hydrogen bonds formed within piperidine molecules.

3.5. NMR spectroscopy

Fig. 5 displays the ^{1}H NMR spectrum of the mixture of C_{70} and pip in 1,2-dichlorobenzene. The spectra of pure C_{70} and piperidine, and the mixture of C_{60} with pip in the same solvent are shown for comparison. In agreement with the previously studied $C_{60}\cdots$pip system (Fig. 5 and ref. 27), the character of the spectrum at the chemical shift of about 3.5 ppm also changes in the $C_{70}\cdots$pip mixture, however, in a more complex manner. Based on the previous study on $C_{60}\cdots$pip in 1,2-dichlorobenzene,[27] the observed changes are interpreted by forming the N→C bond. A larger number of the new signals and lower intensities (Fig. 5) most likely result from the lower symmetry of C_{70} compared to C_{60}, hence a presence of multiple complexes. However, the observed experimental results cannot

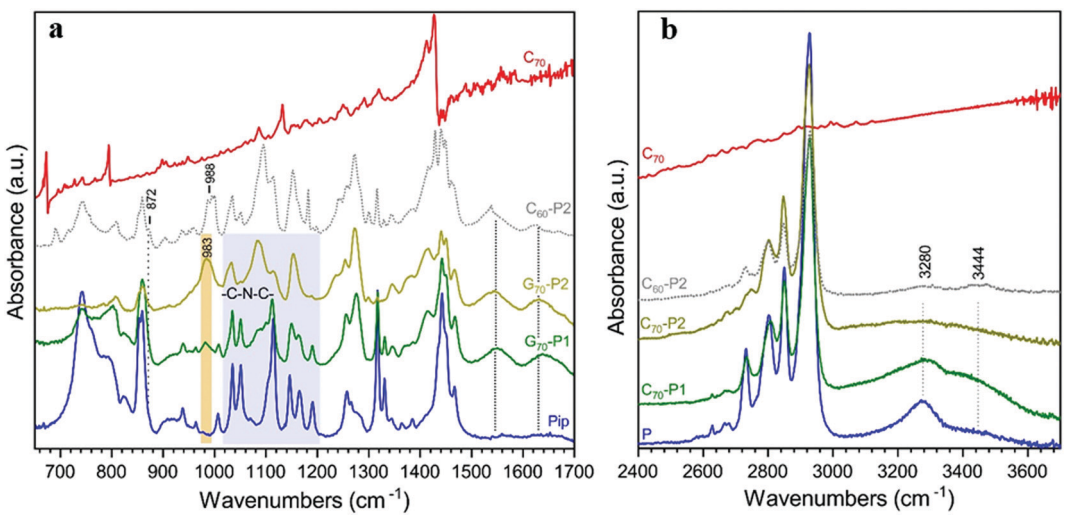

Fig. 4 FT-IR spectra of C_{70} and its complex with piperidine before evaporation (C_{70}-P1) and after evaporation of some excess amount of unbound piperidine molecules (C_{70}-P2) at two spectral windows for the observation of (a) the C-N stretching and N-H bending vibrations, and (b) the N–H stretching vibrations. The spectra of pure piperidine and its complexes with C_{60} (C_{60}-P2) are given for comparison.[27]

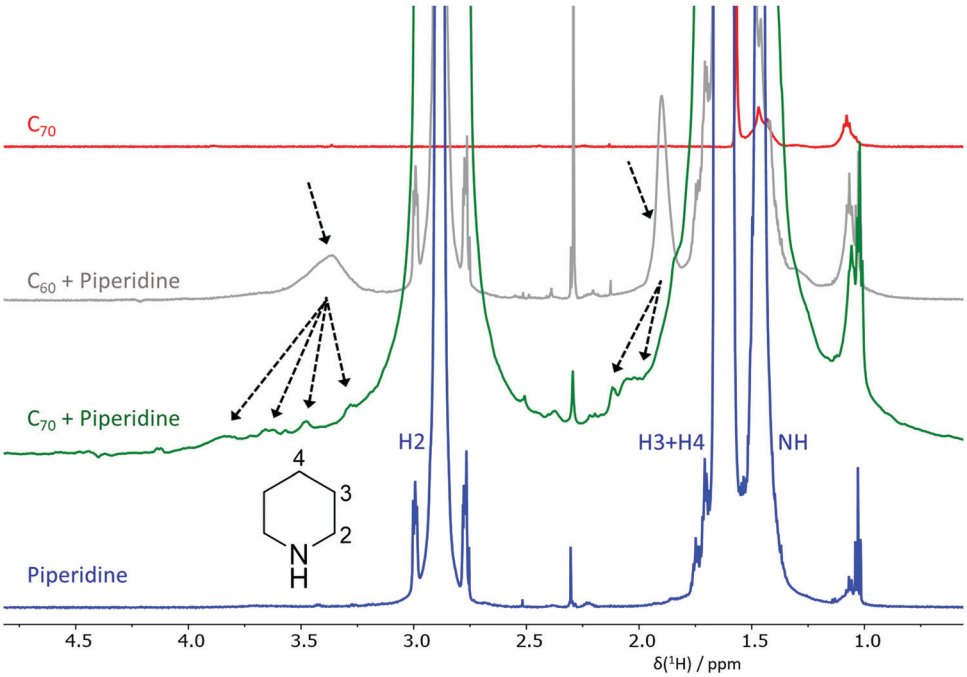

Fig. 5 Part of ^{1}H NMR spectra of 1,2-dichlorobenzene-d4 (550 μL) solutions of piperidine, the mixture of C_{70} and piperidine, the mixture of C_{60} and piperidine, and C_{70}. The black dashed arrows highlight the signals of the C_{60}-piperidine and C_{70}-piperidine complexes.

provide a conclusive answer to whether the different signals result from binding of the inner pip to various sites or from a different orientation of the outer pip to C_{70}. The calculated ^{1}H-NMR spectra show the larger chemical shifts of C-H hydrogens at alpha-(H2) positions compared to those in the isolated pip. This observation correlates well with the experimental ^{1}H-NMR spectra (Fig. 5). In fact, the equatorial hydrogens in the inner pip show the largest chemical shifts indicating a direct involvement of pip N in the complex compared to the outer pip (Table S4, ESI†).

The low concentration of the complexes does not allow for fast measurement of carbon NMR spectra. However, the proton–carbon correlation experiment (HSQC, Fig. S4, ESI†) shows that the new proton signals are attached to piperidine carbon atoms with similar chemical shifts as those in the previously studied C_{60}-piperidine complex.[27]

Unfortunately, during 1–2 days required to obtained a C-NMR spectrum with a good signal-to-noise ratio (Fig. S5, ESI†), new signals overlapping with the original signals, observed immediately after dissolution, appear in proton spectra (see Fig. S6, ESI†). These new signals probably correspond to the structures resulting after the addition of piperidine to C_{70}. ^{13}C spectrum of the sample after standing (Fig. S5, ESI†) exhibits signals in the region 70–80 ppm, which are typical for the products of addition (*i.e.*, covalent bond formation) of secondary amines to C_{60}.[65]

3.6. Explanation of different strengths of the N→C dative bond at various structural motifs of C_{70}

The above calculations on the interaction energies in $C_{70}\cdots$pip complexes forming N→C bond together with previously reported results on the character of pip complexes with C_{20}, C_{60}, and CNT structures[27] call for further discussion on structural prerequisites of carbon allotropes to form the dative bond with electron-donating systems, and the secondary amines, in particular. The symmetry of C_{70} with binding carbon-sites of different characters, *i.e.*, five different types according to their location within the C_{70} structure, offers a sound system for such analysis. Regardless of the thermodynamic (in)stability of the dative bond complexes, stable $C_{70}\cdots(pip)_2$ minima with N→C bond exist at all three carbon-sites (A, B, and C) of C_{70}, characterized by ΔE^{INTR} and ΔE values in the range of −29 to −40 kcal mol^{-1} and −4 to −16 kcal mol^{-1}, respectively, *i.e.*, with a similar stabilities as $C_{60}\cdots(pip)_2$ DB complexes with ΔE^{INTR} of −36 kcal mol^{-1} and ΔE of −13 kcal mol^{-1}. The failure of CNT to form these complexes led to the conclusion that the out-of-plane planarity is an essential but insufficient requirement to form dative bonds with carbon allotropes due to the still significant aromatic character of the six-membered ring. The presence of the five-membered ring explained the formation of dative bonds due to their larger aromaticity decrease upon deviation from planarity.[27]

Our results on $C_{70}\cdots(pip)_2$ reveal the large stability of DB complexes formed at sites that contain five- and six-member rings (sites A and B). The complex formed on the A-site, located close to apexes of the rugby ball with larger out-of-plane deviation, is more stable (see Fig. 6 and Scheme 1) than that formed on the B-site, located close to the central part of the ball. The existence of the dative bond at the C-site containing only the six-member rings is surprising and contradicts the previously proposed prerequisite to forming the dative bond. Fig. 7 explains the observed DB formation at the C-site based solely on structural arguments. Comparison of the geometries of the pyrene motif cut from CNT, C_{70}, and isolated pyrene

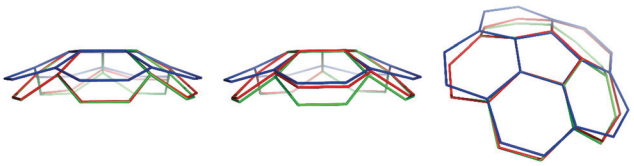

Fig. 6 Curvature comparison of Isolated-pentagon-rule motif (blue), A motif from C_{70} (green), and B motif from C_{70} (red) from three different views.

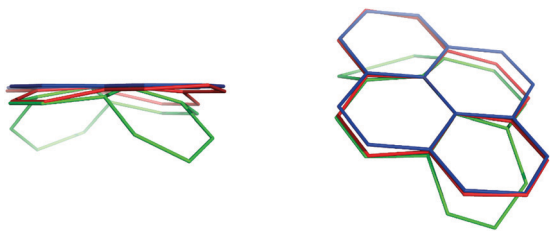

Fig. 7 Comparison of planar pyrene (blue) and pyrene motifs cut from carbon nanotube (red) and C-site of C_{70} (green) viewed from different angles.

shows the trends in structure distortions of the former two systems. While the pyrene motif significantly declines from the plane in one direction in CNT, it deviates from the plane in both directions in the C_{70} fragment.

The stability and chemical reactivity of non-planar π-conjugated systems are described based on the π-orbital axis vector (POAV) analysis.[66–68] For this purpose, the systematic calculations of pyramidalization angles of the carbon atoms at the A, B, and C-sites in C_{70} are performed, giving the values of 11.9°, 11.5°, and 8.6°, respectively. The values for planar benzene and C_{60} are 0° and 11.6°, respectively.[66] This analysis indicates a larger reactivity of the A-site in C_{70} than CNT (m,n), with m = 6–10, n = 0, and CNT (m,m) with m = 5–8. This result further supports the DB complex formation.[68]

Calculations of Fukui indices (f_k^+, see Table S5, ESI†) also reveal different potentials of carbon sites for N→C formation. Larger values of f_k^+ obtained for the A and B sites are in line with their larger interaction energies in DB complexes compared to the smaller stability and small f_k^+ value calculated for the C-site and the inability to form this complex in CNT with the negative value of f_k^+.

Thus, the above analyses conclude that the N→C bond between fullerenes and pip can form at any structural motif providing sufficient out-of-plane deviations.

4. Conclusions

The present studies on the complexes of the secondary amine piperidine and C_{70} performed using computational modeling and experimental IR and NMR spectroscopy prove the dative/covalent complex's existence, previously observed for other ball-shaped carbon allotropes, and provide additional insight into its structural selectivity. Larger out-of-plane deviations occurred in both directions of the pyrene fragment explain the dative bond formation at the region with six-membered rings, not observed previously with CNT. The calculations reveal stronger bonding on carbon sites which participate in both, five- and six-member rings compared to carbon site located in the region consisting solely of six-member rings. The calculated free energies suggest that only the complexes formed with carbon sites on the poles of the rugby-ball structure are thermodynamically stable. This study provides previously unknown information on the interaction of C_{70} with secondary amines, which may be exploited to design fullerene derivatives with application in spintronics, (electro)catalysis, and energy storage.

Conflicts of interest

The authors declare no competing financial interest.

Acknowledgements

M. L. acknowledges the Palacký University Internal Grant Association (IGA_PrF_2020_022). W. W. gratefully acknowledges the National Science Foundation of China (21773104) for funding. The support of the Czech Science Foundation, the projects 19-27454X (R. L., D. N., A. B., D. M., R. Z., and P. H.) and 18-11851S (M.D.) is also acknowledged. We thank Tomáš Steklý for technical assistance in sample preparation and FT-IR data collection.

References

1 D. Jović, V. Jaćević, K. Kuča, I. Borišev, J. Mrdjanovic, D. Petrovic, M. Seke and A. Djordjevic, The Puzzling Potential of Carbon Nanomaterials: General Properties, Application, and Toxicity, *Nanomaterials*, 2020, **10**, 1508.
2 J. Joseph, V. S. Sivasankarapillai, S. Nikazar, M. S. Shanawaz, A. Rahdar, H. Lin and G. Z. Kyzas, Borophene and Boron Fullerene Materials in Hydrogen Storage: Opportunities and Challenges, *ChemSusChem*, 2020, **13**, 3754–3765.
3 E. I. Pochkaeva, N. E. Podolsky, D. N. Zakusilo, A. V. Petrov, N. A. Charykov, T. D. Vlasov, A. V. Penkova, L. V. Vasina, I. V. Murin, V. V. Sharoyko and K. N. Semenov, *Prog. Solid State Chem.*, 2020, **57**, 100255.
4 X. Zhang, H. Cong, B. Yu and Q. Chen, Recent Advances of Water-Soluble Fullerene Derivatives in Biomedical Applications, *Mini-Rev. Org. Chem.*, 2018, **16**, 92–99.
5 L. Jia, M. Chen and S. Yang, Functionalization of fullerene materials toward applications in perovskite solar cells, *Mater. Chem. Front.*, 2020, **4**, 2256–2282.
6 T. Xu, W. Shen, W. Huang and X. Lu, Fullerene micro/nanostructures: controlled synthesis and energy applications, *Mater. Today Nano*, 2020, **11**, 100081.
7 X. Meng, W. Zhang, Z. Tan, Y. Li, Y. Ma, T. Wang, L. Jiang, C. Shu and C. Wang, Highly Efficient and Thermally Stable Polymer Solar Cells with Dihydronaphthyl-Based

[70]Fullerene Bisadduct Derivative as the Acceptor, *Adv. Funct. Mater.*, 2012, **22**, 2187–2193.

8 D. M. Cox, S. Behai, M. Disko, S. M. Gorun, M. Greaney, C. S. Hsu, E. B. Kollin, J. Millar, J. Robbins, W. Robbins, R. D. Sherwood and P. Tindall, Characterization of C_{60} and C_{70} Clusters, *J. Am. Chem. Soc.*, 1991, **113**, 2940–2944.

9 H. Ajie, M. M. Alvarez, S. J. Anz, R. D. Beck, F. Diederich, K. Fosliropoulos, D. R. Huffman, W. Kratschmer, Y. Rubin, K. E. Schriver, D. Sensharma and R. L. Whetten, Characterization of the Soluble All-Carbon Molecules C_{60} and C_{70}, *J. Phys. Chem.*, 1990, **94**, 8630–8633.

10 J. W. Arbogast and C. S. Foote, Photophysical Properties of C_{70}, *J. Am. Chem. Soc.*, 1991, **113**, 8886–8889.

11 J. Baker, P. W. Fowler, P. Lazzeretti, M. Malagoli and R. Zanasi, Structure and properties of C_{70}, *Chem. Phys. Lett.*, 1991, **184**, 182–186.

12 T. Kubo, E. Kanao, T. Matsumoto, T. Naito, T. Sano, M. Yan and K. Otsuka, Specific Intermolecular Interactions by the Localized π-Electrons in C_{70}-fullerene, *ChemistrySelect*, 2016, **1**, 5900–5904.

13 K. Hedberg, L. Hedberg, M. Bühl, D. S. Bethune, C. A. Brown and R. D. Johnson, Molecular Structure of Free Molecules of the Fullerene C_{70} from Gas-Phase Electron Diffraction, *J. Am. Chem. Soc.*, 1997, **119**, 5314–5320.

14 O. A. Troshina, P. A. Troshin, A. S. Peregudov, V. I. Kozlovski and R. N. Lyubovskaya, $C_{70}[NR_2]_2O$: The First C_{70} Intramolecular Ethers Bearing Two Amine Groups, *European*, *J. Org. Chem.*, 2006, 5243–5248.

15 Y. Li, D. Xu and L. Gan, Selective Multiamination of C_{70} Leading to Curved π Systems with 60, 58, 56, and 50 π Electrons, *Angew. Chem., Int. Ed.*, 2016, **55**, 2483–2487.

16 A. Herrmann, M. W. Rüttimann, T. Gibtner, C. Thilgen, F. Diederich, T. Mordasini and W. Thiel, Achiral and chiral higher adducts of C_{70} by Bingel cyclopropanation, *Helv. Chim. Acta*, 1999, **82**, 261–289.

17 W. W. H. Wong and F. Diederich, Regio- and Diastereoselective Synthesis of Bis- and Tetrakisadducts of C_{70} by Directed Remote Functionalization Using Tröger Base Tethers, *Chem. – Eur. J.*, 2006, **12**, 3463–3471.

18 V. S. P. K. Neti, M. R. Cerón, A. Duarte-Ruiz, M. M. Olmstead, A. L. Balch and E. Luis, High-yield, regiospecific bis-functionalization of C_{70} using a Diels–Alder reaction in molten anthracene, *Chem. Commun.*, 2014, **50**, 10584–10587.

19 S. Vidal, M. Izquierdo, W. K. Law, K. Jiang, S. Filippone, J. Perles, H. Yan and N. Martín, Photochemical site-selective synthesis of [70]methanofullerenes, *Chem. Commun.*, 2016, **52**, 12733–12736.

20 M. R. Cerón, M. Izquierdo, A. Aghabali, J. A. Valdez, K. B. Ghiassi, M. M. Olmstead, A. L. Balch, F. Wudl and L. Echegoyen, Tethered Bisadducts of C_{60} and C_{70} with Addends on a Common Hexagonal Face and a 12-Membered Hole in the Fullerene Cage, *J. Am. Chem. Soc.*, 2015, **137**, 7502–7508.

21 A. Aghabali, S. Jun, M. M. Olmstead and A. L. Balch, Piperazine Functionalization of C_{70} for Incorporation into Supramolecular Assemblies, *Chem. – Eur. J.*, 2016, **22**, 18908–18915.

22 C. Thilgen and F. Diederich, The Higher Fullerenes: Covalent Chemistry and Chirality, in *Fullerenes and Related Structures*, ed. A. Hirsch, Topics in Current Chemistry, Springer, Berlin, Heidelberg, 1999, pp. 135–171.

23 H. L. Hou, Z. J. Li, T. Sun and X. Gao, Preparation of a C_{70} Bis-heterocyclic Derivative with High Chemio- and Regioselectivity, *J. Org. Chem.*, 2015, **80**, 5315–5319.

24 P. Jin, L. Yang, C. Liu, M. Chen, Q. Hou, L. Li and Y. Zhao, A comparative study on the N-heterocyclic carbene adducts of I_h-C_{60}, D_{5h}-C_{70} and $Sc_3N@I_h$-C_{80}, *Phys. Chem. Chem. Phys.*, 2017, **19**, 17598–17606.

25 K. Liosi, A. Romero-Rivera, O. Semivrazhskaya, C. D. Caniglia, M. Garcia-Borràs, N. Trapp, S. Osuna and Y. Yamakoshi, Site-Selectivity of Prato Additions to C_{70}: Experimental and Theoretical Studies of a New Thermodynamic Product at the *dd*-[5,6]-Junction, *Org. Lett.*, 2019, **21**(13), 5162–5166.

26 M. Saito, H. Shinokubo and H. Sakurai, Figuration of bowl-shaped π-conjugated molecules: properties and functions, *Mater. Chem. Front.*, 2018, **2**, 635–661.

27 M. Lamanec, R. Lo, D. Nachtigallová, A. Bakandritsos, E. Mohammadi, M. Dračínský, R. Zbořil, P. Hobza and W. Wang, The Existence of a N→C Dative Bond in the C_{60}–Piperidine Complex, *Angew. Chem., Int. Ed.*, 2021, **60**, 1942–1950.

28 E. Kleinpeter, S. Klod and A. Koch, Endohedral and external through-space shieldings of the fullerenes C_{50}, C_{60}, C_{60}^{6-}, C_{70}, and C_{70}^{6-} – Visualization of (anti)aromaticity and their effects on the chemical shifts of encapsulated nuclei, *J. Org. Chem.*, 2008, **73**, 1498–1507.

29 E. F. Sheka, 'Chemical portrait' of fullerene molecules, *J. Struct. Chem.*, 2006, **47**, 593–599.

30 E. Chamorro, P. Pérez and L. R. Domingo, On the nature of Parr functions to predict the most reactive sites along organic polar reactions, *Chem. Phys. Lett.*, 2013, **582**, 141–143.

31 L. R. Domingo, P. Pérez and J. A. Sáez, Understanding the local reactivity in polar organic reactions through electrophilic and nucleophilic Parr functions, *RSC Adv.*, 2013, **3**, 1486–1494.

32 W. Yang and W. J. Mortier, The Use of Global and Local Molecular Parameters for the Analysis of the Gas-Phase Basicity of Amines, *J. Am. Chem. Soc.*, 1986, **108**, 5708–5711.

33 S. L. Wu, Z. J. Li and X. Gao, Dithiolation of [70]Fullerene with Aliphatic Primary Thiols in the Presence of *n*-Butylamine via Aerobic Oxidation Reaction, *J. Org. Chem.*, 2019, **84**, 3045–3054.

34 S. H. Li, Z. J. Li, W. W. Yang and X. Gao, Controlled Synthesis of C_{70} Equatorial Multiadducts with Mixed Addends from an Equatorial Diadduct: Evidence for an Electrophilic Carbanion, *Org. Lett.*, 2018, **20**, 2328–2332.

35 M. Li, X. He, B. Wang, D. Zhao, C. Rong, P. K. Chattaraj and S. Liu, Changes in Structure and Reactivity of Ng2 Encapsulated in Fullerenes: A Density Functional Theory Study, *Front. Chem.*, 2020, **8**, 566.

36 C. Adamo and V. Barone, Toward reliable density functional methods without adjustable parameters: The PBE0 model, *J. Chem. Phys.*, 1999, **110**, 6158–6170.

37 S. Grimme, J. Antony, S. Ehrlich and H. Krieg, A consistent and accurate ab initio parametrization of density functional dispersion correction (DFT-D) for the 94 elements H-Pu, *J. Chem. Phys.*, 2010, **132**, 154104.
38 S. Grimme, S. Ehrlich and L. Goerigk, Effect of the damping function in dispersion corrected density functional theory, *J. Comput. Chem.*, 2011, **32**, 1456–1465.
39 F. Weigend, Hartree-fock exchange fitting basis sets for H to Rn, *J. Comput. Chem.*, 2008, **29**, 167–175.
40 M. J. Frisch, G. W. Trucks, H. B. Schlegel, G. E. Scuseria, M. A. Robb, J. R. Cheeseman, G. Scalmani, V. Barone, G. A. Petersson, H. Nakatsuji, X. Li, M. Caricato, A. Marenich, J. Bloino, B. G. Janesko, R. Gomperts, B. Mennucci, H. P. Hratchian, J. V. Ortiz, A. F. Izmaylov, J. L. Sonnenberg, D. Williams-Young, F. Ding, F. Lipparini, F. Egidi, J. Goings, B. Peng, A. Petrone, T. Henderson, D. Ranasinghe, V. G. Zakrzewski, J. Gao, N. Rega, G. Zheng, W. Liang, M. Hada, M. Ehara, K. Toyota, R. Fukuda, J. Hasegawa, M. Ishida, T. Nakajima, Y. Honda, O. Kitao, H. Nakai, T. Vreven, K. Throssell, J. A. Montgomery, Jr., J. E. Peralta, F. Ogliaro, M. Bearpark, J. J. Heyd, E. Brothers, K. N. Kudin, V. N. Staroverov, T. Keith, R. Kobayashi, J. Normand, K. Raghavachari, A. Rendell, J. C. Burant, S. S. Iyengar, J. Tomasi, M. Cossi, J. M. Millam, M. Klene, C. Adamo, R. Cammi, J. W. Ochterski, R. L. Martin, K. Morokuma, O. Farkas, J. B. Foresman and D. J. Fox, *Gaussian 09, Revision D.01*, Gaussian, Inc., Wallingford CT, 2016.
41 A. Klamt, G. Schüürmann and COSMO, A New Approach to Dielectric Screening in Solvents with Explicit Expressions for the Screening Energy and Its Gradient, *J. Chem. Soc., Perkin Trans. 2*, 1993, 799–805.
42 J. D. Chai and M. Head-Gordon, Long-Range Corrected Hybrid Density Functionals with Damped Atom-Atom Dispersion Corrections, *Phys. Chem. Chem. Phys.*, 2008, **10**, 6615–6620.
43 F. Weigend and R. Ahlrichs, Balanced Basis Sets of Split Valence, Triple Zeta Valence and Quadruple Zeta Valence Quality for H to Rn: Design and Assessment of Accuracy, *Phys. Chem. Chem. Phys.*, 2005, **7**, 3297–3305.
44 K. Wolinski, J. F. Hinton and P. Pulay, Efficient implementation of the gauge-independent atomic orbital method for NMR chemical shift calculations, *J. Am. Chem. Soc.*, 1990, **112**, 8251–8260.
45 M. Kaupp, M. Behl and V. G. Malkin, *Calculation of NMR and EPR Parameters: Theory and Applications*, Wiley-VCH, Weinheim, 2004.
46 J. Kaminský, M. Buděšínský, S. Taubert, P. Bouř and M. Straka, Fullerene C_{70} characterization by ^{13}C NMR and the importance of the solvent and dynamics in spectral simulations, *Phys. Chem. Chem. Phys.*, 2013, **15**, 9223–9230.
47 R. M. Parrish, L. A. Burns, D. G. A. Smith, A. C. Simmonett, A. E. DePrince, E. G. Hohenstein, U. Bozkaya, A. Y. Sokolov, R. Di Remigio, R. M. Richard, J. F. Gonthier, A. M. James, H. R. McAlexander, A. Kumar, M. Saitow, X. Wang, B. P. Pritchard, P. Verma, H. F. Schaefer, K. Patkowski, R. A. King, E. F. Valeev, F. A. Evangelista, J. M. Turney, T. D. Crawford and C. D. Sherrill, Psi4 1.1: An Open-Source Electronic Structure Program Emphasizing Automation, Advanced Libraries, and Interoperability, *J. Chem. Theory Comput.*, 2017, **13**, 3185–3197.
48 MOPAC2016, James J. P. Stewart, Stewart Computational Chemistry, Colorado Springs, CO, USA, http://OpenMOPAC.net, 2016.
49 J. Řezáč, Cuby: An integrative framework for computational chemistry, *J. Comput. Chem.*, 2016, **37**, 1230–1237.
50 A. Pecina, S. Haldar, J. Fanfrlík, R. Meier, J. Řezáč, M. Lepšík and P. Hobza, SQM/COSMO Scoring Function at the DFTB3-D3H4 Level: Unique Identification of Native Protein-Ligand Poses, *J. Chem. Inf. Model.*, 2017, **57**, 127–132.
51 H. J. C. Berendsen, J. P. M. Postma, W. F. Van Gunsteren, A. Dinola and J. R. Haak, Molecular dynamics with coupling to an external bath, *J. Chem. Phys.*, 1984, **81**, 3684–3690.
52 F. Neese, A. Hansen and D. G. Liakos, Efficient and Accurate Approximations to the Local Coupled Cluster Singles Doubles Method Using a Truncated Pair Natural Orbital Basis, *J. Chem. Phys.*, 2009, **131**, 064103.
53 F. Neese, A. Hansen, F. Wennmohs and S. Grimme, Accurate Theoretical Chemistry with Coupled Pair Models, *Acc. Chem. Res.*, 2009, **42**, 641.
54 W. B. Schneider, G. Bistoni, M. Sparta, M. Saitow, C. Riplinger, A. A. Auer and F. Neese, Decomposition of Intermolecular Interaction Energies within the Local Pair Natural Orbital Coupled Cluster Framework, *J. Chem. Theory Comput.*, 2016, **12**, 4778.
55 A. Bauzá, T. J. Mooibroek and A. Frontera, Tetrel-bonding interaction: Rediscovered supramolecular force?, *Angew. Chem., Int. Ed.*, 2013, **52**, 12317–12321.
56 A. M. S. Riel, R. K. Rowe, E. N. Ho, A. C. C. Carlsson, A. K. Rappé, O. B. Berryman and P. S. Ho, Hydrogen Bond Enhanced Halogen Bonds: A Synergistic Interaction in Chemistry and Biochemistry, *Acc. Chem. Res.*, 2019, **52**, 2870–2880.
57 G. A. Jeffrey, Hydrogen-Bonding: An update, *Crystallogr. Rev.*, 2003, **9**, 135–176.
58 S. Toyota, Y. Yamamoto, K. Wakamatsu, E. Tsurumaki and A. Muñoz-Castro, Nano-Saturn with an Ellipsoidal Body: Anthracene Macrocyclic Ring–C_{70} Complex, *Bull. Chem. Soc. Jpn.*, 2019, **92**, 1721–1728.
59 J. Calbo, R. Viruela, E. Ortí and J. Aragó, Relationship between Electron Affinity and Half-wave Reduction Potential: A Theoretical Study on Cyclic Electron-Acceptor Compounds, *Chem. Phys. Chem.*, 2016, **17**, 3881–3890.
60 J. C. Gonzalez, S. Mondal, F. Ocayo, R. Guajardo-Maturana and A. Muñoz-Castro, Nature of C60 and C70 Fullerene Encapsulation in a Porphyrin-and Metalloporphyrin-Based Cage. Insights from Dispersion Corrected DFT Calculations, *Int. J. Quantum Chem.*, 2020, **120**, e26080.
61 C. O. Ulloa, M. Ponce-Vargas and A. Muñoz-Castro, Formation of Coinage-Metal···Fullerene Adducts. Evaluation of the Interaction Nature between Triangular Coinage Metal

Complexes (M3 = Cu, Ag, and Au) and C60 through Relativistic Density Functional Theory Calculations, *J. Phys. Chem. C*, 2018, **122**, 25110–25117.

62 D. Chen, D. W. Szczepanik, J. Zhu, A. Muñoz-Castro and M. Solà, Aromaticity Survival in Hydrofullerenes: The Case of $C_{66}H_4$ with Its π-Aromatic Circuits, *Chem. – Eur. J.*, 2021, **27**, 802–808.

63 P. Larkin, *Infrared and Raman Spectroscopy: Principles and Spectral Interpretation*, Elsevier, Waltham, MA, USA, 2011.

64 Y. S. Mary, H. T. Varghese, C. Y. Panicker, M. Girisha, B. K. Sagar, H. S. Yathirajan, A. A. Al-Saadi and C. Van Alsenoy, Vibrational spectra, HOMO, LUMO, NBO, MEP analysis and molecular docking study of 2,2-diphenyl-4-(piperidin-1-yl)butanamide, *Spectrochim. Acta, Part A*, 2015, **150**, 543–556.

65 Y. Li and L. Gan, Selective Addition of Secondary Amines to C_{60}: Formation of Penta- and Hexaamino[60]fullerenes, *J. Org. Chem.*, 2014, **79**, 8912–8916.

66 R. C. Haddon, Chemistry of the Fullerenes: The Manifestation of Strain in a Class of Continuous Aromatic Molecules, *Science*, 1993, **261**, 1545–1550.

67 K. H. Lee, C. Lee, J. Kang, S. S. Park, J. Lee, S. K. Lee and D. K. Bohme, Preferential Site of Attack on Fullerene Cations: Frontier Orbitals and Rate Coefficients, *J. Phys. Chem. A*, 2006, **110**, 11730–11733.

68 B. Hong-Cun, Z. Ying, Y. Ni-Ni, J. Yong-Qiang, Q. Wei-Ye and H. Yuan-He, New Solution Method of Pi-Orbital Axis Vector and Its Applications in Fullerenes and Carbon Nanotubes, *Chin. J. Struct. Chem.*, 2013, **32**, 695–703.